RSC Advances

PAPER

View Article Online
View Journal | View Issue

Cite this: *RSC Adv.*, 2021, **11**, 10340

Environmental investigation of pollutants in coal mine operation and waste dump area monitored in Ordos Region, China

Ang Li,[ab] Changkun Chen,*[a] Jie Chen[a] and Peng Lei[a]

The increasingly severe emissions of greenhouse and poisonous gases from environmentally unsafe stockpiled coal mine waste dumps have urged people from the academia as well as the industry to focus on environmental impact assessment. In this study, one-year air pollutant monitoring was conducted at the Qipanjing coalfield in Inner Mongolia of China for determining the distribution pattern statue of pollutant exposure and its main driving factors. We used FTIR spectroscopy to measure the inorganic compounds in particulate matter with a diameter of less than 2.5 μm. The spatial and temporal distribution characteristics of leading pollutants, including $PM_{2.5}$, PM_{10}, SO_2, NO_2, O_3 and CO were analyzed. Firstly, the research showed that the temporal and spatial distribution of pollutants in the coal mine waste area is non-homogeneous. Secondly, some meteorological parameters, such as wind speed, relative humidity, temperature, and rainfall, were found to have significant effects on air pollutant distribution. Stable atmospheric conditions were unfavorable for the diffusion of pollutants and prolong the pollution process. Finally, in the vicinity of coalfields, SO_2 and NO_2 are present in high concentrations in air. Primary reasons for such high values are coal mining-related activities and active mine fires. This study will help to offer valuable and detailed information for understanding and interpreting the pollution source.

Received 17th December 2020
Accepted 24th February 2021

DOI: 10.1039/d0ra10586d

rsc.li/rsc-advances

1. Introduction

The increasingly severe environmental pollution problems, such as haze and poisonous gas dust usually induced by coal mine waste fires from coal industrial processes, have gained an increasing amount of attention from both the academia and the industry.[1] With the multiple release sources and multiple channels of active coalfield fires, it is difficult to control and eliminate toxic gases produced. Coalfield fires not only lead to severe air pollution but also pose a great threat to the residents of the mining area.[2–4] Coal fires, which can happen in any coal producing country all over the world at any time, have resulted in damage to the atmospheric environment, which has evolved into a global disaster. Coal mine fires have been reported in China, India, the United States, Australia, Russia, Indonesia, Venezuela, South Africa, and other countries.[5] A large number of opencast coal mines are distributed in the central and western region of China. The coal spontaneous combustion in coalfields is extremely common, particularly in the middle reaches of the Yellow River. The combustion of coal in the mining area could produce a large quantity of toxic gases, which can pollute the environment. According to the statistical data, the spontaneous combustion of coal seams and coal waste piles releases a lot of CO, SO_2, H_2S, NO_X, benzopyrene, and other noxious and detrimental gases.[6–8] Meanwhile, it has been proved that the content of Pb, Cr, Hg, F, and As in the emitted flue gas exceeded the industrial pollution standard in Inner Mongolia.[4,6]

The severity of coal mine fires was disclosed and the origin of coal mine fires and related gases was described by Stracher.[9] Many coal seams or gangue hills are piled up, which not only occupy land but also pollute the surrounding soil and groundwater. Spontaneous combustion and explosion would take place under the appropriate conditions of temperature exceeding approximately 80 °C and coal accumulation.[10] This produces high pressure, high-temperature heat waves, dust, and shock waves, and most importantly, releases greenhouse and toxic gases to affect the health of residents in the mining area.[11,12]

Recent studies have mainly focused on the simulations of mercury and carbon emissions from coal seam fires.[13] The distribution of the pollution sources, topography, and meteorological factors in the mining area would lead to a difference in the spatial and temporal distribution of atmospheric pollution. The temporal and spatial distribution of atmospheric pollution has a distinctive regional characteristic, and the temporal and spatial distribution of different pollutants varies considerably.[14] Therefore, the research on air pollutant monitoring in coal mining areas is vital because it can be used to assess the

[a]*Institute of Disaster Prevention Science and Safety Technology, Central South University, Changsha, 410075, China. E-mail: cckchen@csu.edu.cn*
[b]*College of Forestry, Inner Mongolia Agricultural University, Hohhot, 010019, China*

potential hazards and combined effects to determine short-term and long-term pollutant dispersion, and to improve the relevant assessment standards and regulations of air quality.[14,15]

The research on air pollutant monitoring is of great significance to guide air quality management efforts, to assess potential comprehensive effects, to reasonably allocate the possible emission sources, to determine the short-term and long-term migration of pollutants, and to improve air quality control laws and regulations. In addition, mining and its related activities, such as near the railway branch line, burning coal in the open air, and heavy vehicle load, are the main reasons for the high concentration of air pollutants in coalfields.[16] The method of spatio-temporal interpolation for air quality data was applied to the daily nitric oxide concentration measurement of monitoring stations around the city, and the temporal and spatial variability of NO observations could be analyzed.[17,18] The geostatistical characterization of the nitrogen dioxide concentration in an urban area was mapped by the co-Kriging method to improve the estimation of seasonal or annual concentrations.[19] The metal composition released by a forest fire is similar to that released by a coal fire.[20] Numerous studies have focused on the spatial and temporal variations of primary fine particles with diameters smaller than 10 μm (PM_{10}) and 2.5 μm ($PM_{2.5}$), and harmful gases such as sulphur dioxide (SO_2), nitrogen oxides (NOx), ammonia (NH_3), and volatile organic compounds (VOCs).[11,13–15,21] Substantial seasonal differences and long-term trends of air pollutant levels have been noticed in several regions around the world.[22–24] The seasonal and trend disparities among the cities could be caused by several factors, including the diffusion of local pollution sources, the existence of distant pollution sources affecting the city, and the meteorological and topographical conditions of the area.[25,26] Although previous studies have tried to give some data about potential gas emissions during coal mine fires, these studies have focused on underground coal mine fires. This paper mainly studies environmental pollution in the process of coal mine fire activities in coalfield fire areas, and determines the pollution sources of coal mine fire and their influences. This also provides some ideas for the management strategy of the Chinese government to limit the pollution in the coalfield fire area.

The present study was conducted based on the one-year study of 2018 air pollutant concentration monitoring the coal mine waste area in the Qipanjing town of the Inner Mongolia Autonomous Region, China. The aim of this study is to describe the origin of coal fires and related gases, such as PM_{10}, $PM_{2.5}$, NO_2, SO_2, CO, and O_3, to explore the spatiotemporal variations, statistical distributions, and conventional air pollutants emitted by coal mine fires, and to analyze the influencing factors of the spatial and temporal emission distribution.

2. Materials and methods

2.1 Study area

The heavy industry gathering area in Ordos Region was selected as the study area, including Mengxi Industrial Park and Qipanjing Economic Development Zone, in which there are some large-scale industrial enterprises and power plants with serious pollution. It is located at 39°22′32″ north latitude and 107°00′44″ east longitude, and belong to a typical temperate continental monsoon climate. Moreover, it is a crucial traffic hub of the Ordos City, connecting the Ningxia Hui Autonomous Region and the Wuhai City. The entire planned area of the industrial zone is 85 square kilometres. The integral area of Qipanjing Town is 3614 square kilometres and the total population was 82 000 at the end of 2018.

The annual sunshine hours are about 3000 hours, the annual average temperature is about 6.4 °C, the annual precipitation is about 250 mm, and the annual evaporation is about 3000 mm. The precipitation is mainly concentrated in July–September and the frost-free period is over 122 days.[27] In particular, natural climatic conditions such as drought, frequent wind, and strong sunshine, provide the necessary conditions in this area that lead to a frequent occurrence of coal fires.

Based on the principle of convenient scheduling and sampling, six different sites were selected as the monitoring points of the air quality in the coalfield fire area to analyze the air pollution status. The location of monitoring points is shown in Fig. 1.

We used the micro-air quality sensors Microair A108, which are supplied by Fairsense (Beijing) Environmental Technology Co. Ltd, to measure PM_{10}, $PM_{2.5}$, SO_2, NO_2, O_3, CO, temperature, humidity, and other parameters in the atmosphere. According to the ambient air quality standard GB3095-2012 (MEP, 2012), the pollutant concentration was calculated using the following methods. The NO_2 concentration was determined by chemiluminescence and differential optical absorption spectroscopy (DOAS). In addition, UV fluorescence and DOAS were used for the determination of SO_2 concentration. Ultraviolet absorption spectroscopy and DOAS determined the concentration of O_3. The CO concentration was measured by the filtered infrared and non-dispersive infrared absorption methods. The measurement of the mass concentration of PM was conducted by the cone element oscillating microbalance and the gamma-ray method.

Samples of $PM_{2.5}$ were collected on filters of HUCM, QCB, XCWP, and FODS monitoring sites at four sites. In a volume sampler at the inlet of $PM_{2.5}$, $PM_{2.5}$ aerosol was collected on a 3 cm × 3 cm glass fiber filter at a speed of 16.7 L min^{-1} (once every 4 hours). The drug NH_4NO_3 used in the experiment was analytically pure. The sampling period is from January 20, 2018 to January 25, 2018. In this experiment, all the samples were analyzed using a Fourier-transform infrared spectrometer (Thermo Nicolet 380) with smart single-bounce ATR and multiple-bounce ATR. The wavenumber of the sample spectrum is 400–4000 cm^{-1} and the resolution is 4 cm^{-1}. By measuring the infrared spectrum of the sample film on the whole substrate, the linear relationship between the mass of sulfate, nitrate, and ammonium ions and its absorbance is established, and calibration is realized.

2.2 Data description and methods

The temporal heterogeneity data of the ruling air pollutants were analyzed and compared in terms of the dominant days of each pollutant. The number of days with PM_{10} as the dominant

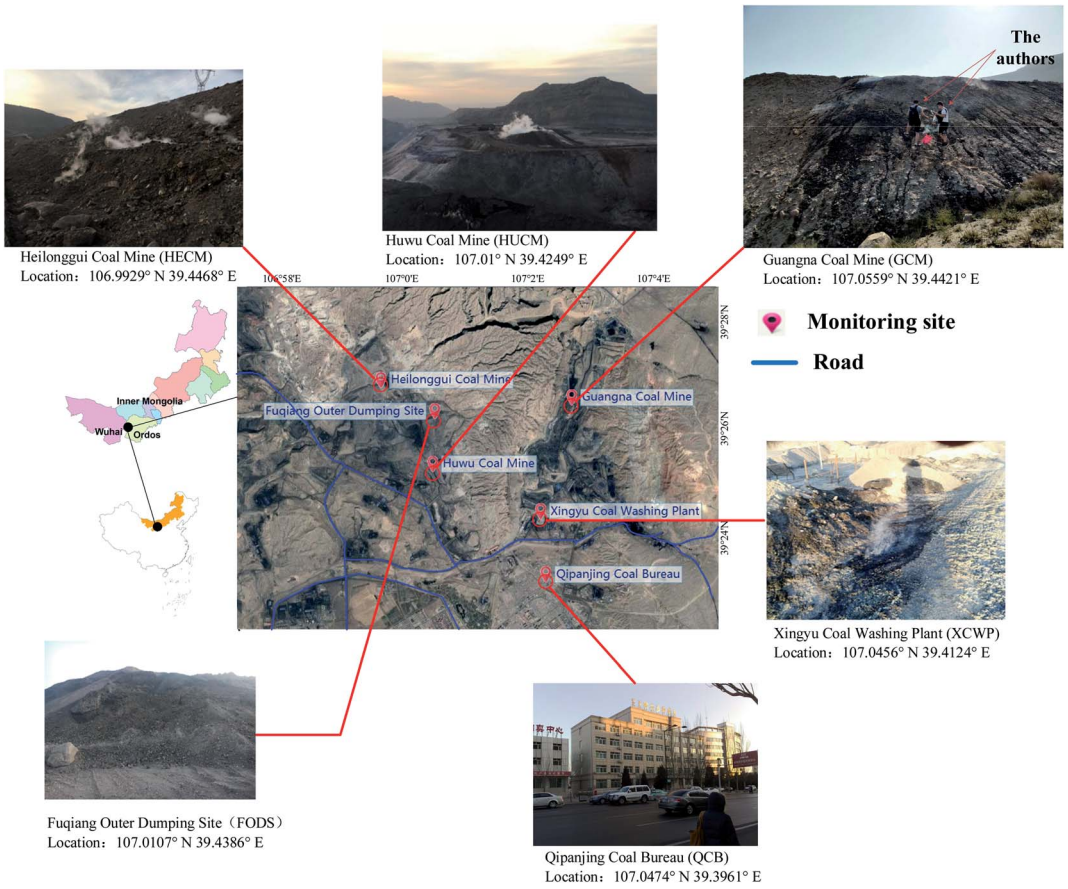

Fig. 1 Location of monitoring sites in the study area in 2018.

air pollutant was more than 80, which was the greatest among all the pollution days in spring at all the six sites. The number of days with $PM_{2.5}$ as the dominant air pollutant was more than 68, which was the largest among all the pollution days in winter at all the sites. The sum of days on which SO_2 was the dominant air pollutant was more than 20, which was the largest among all the seriously polluted days at each site in winter and spring.

The Air Quality Index (AQI) was calculated using the following formula:

$$I = \frac{I_{high} - I_{low}}{C_{high} - C_{low}}(C - C_{low}) + I_{low} \quad (1)$$

where I = AQI, C = contaminant concentration, C_{low} = limited value less than or equal to C, C_{high} = limited value higher than or equal to C, I_{low} = limited index of AQI corresponding to C_{low}, and I_{high} = limited index of AQI corresponding to C_{high}.

The correlation coefficient was defined as follows:

$$r = \frac{\sum_{i=1}^{n}\left(X_i - \overline{X}\right)\left(Y_i - \overline{Y}\right)}{\sqrt{\sum_{i=1}^{n}\left(X_i - \overline{X}\right)^2}\sqrt{\sum_{i=1}^{n}\left(Y_i - \overline{Y}\right)^2}} \quad (2)$$

where $\bar{X}$ and $\bar{Y}$ are the average values of X and Y, respectively, and i is the total number of variables. The terms "significant/strong", "moderate", and "insignificant" apply to correlation matrix analysis (CMA).

Principal component analysis (PCA) is a multivariate process, which reduces the dimension of the data sets containing a large number of air pollutant concentrations ($PM_{2.5}$, PM_{10}, SO_2, NO_2, CO, and O_3). Therefore, factor analysis could be used to reduce the dimension of the variable. According to the theory of factor analysis, either of the following equations can be obtained.

$$\begin{bmatrix} F_1 \\ F_2 \\ \cdots \\ F_n \end{bmatrix} = \begin{bmatrix} a_{1,1} & a_{1,2} & \cdots & a_{1,6} \\ a_{2,1} & a_{2,2} & \cdots & a_{2,6} \\ \cdots & \cdots & \cdots & \cdots \\ a_{n,1} & a_{n,2} & \cdots & a_{n,6} \end{bmatrix} \times [PM_{2.5}, PM_{10}, SO_2, NO_2, CO, O_3] \quad (3)$$

where F_i is the ith factor that explains the air pollutants and $a_{i,j}$ is the factor load matrix representing the degree to which jth air pollutants participate in defining F_i. The derivation of factor analysis is based on the normalized linear projection shown in eqn (3).

Through factor analysis, the contribution of various air pollutants to the main factors can be obtained. Therefore, the factor score of the monitoring sites could be calculated using eqn (4)

$$FS_{i,j} = \sum_{k=1}^{6} x_{k,j} FL_{k,i} \quad (4)$$

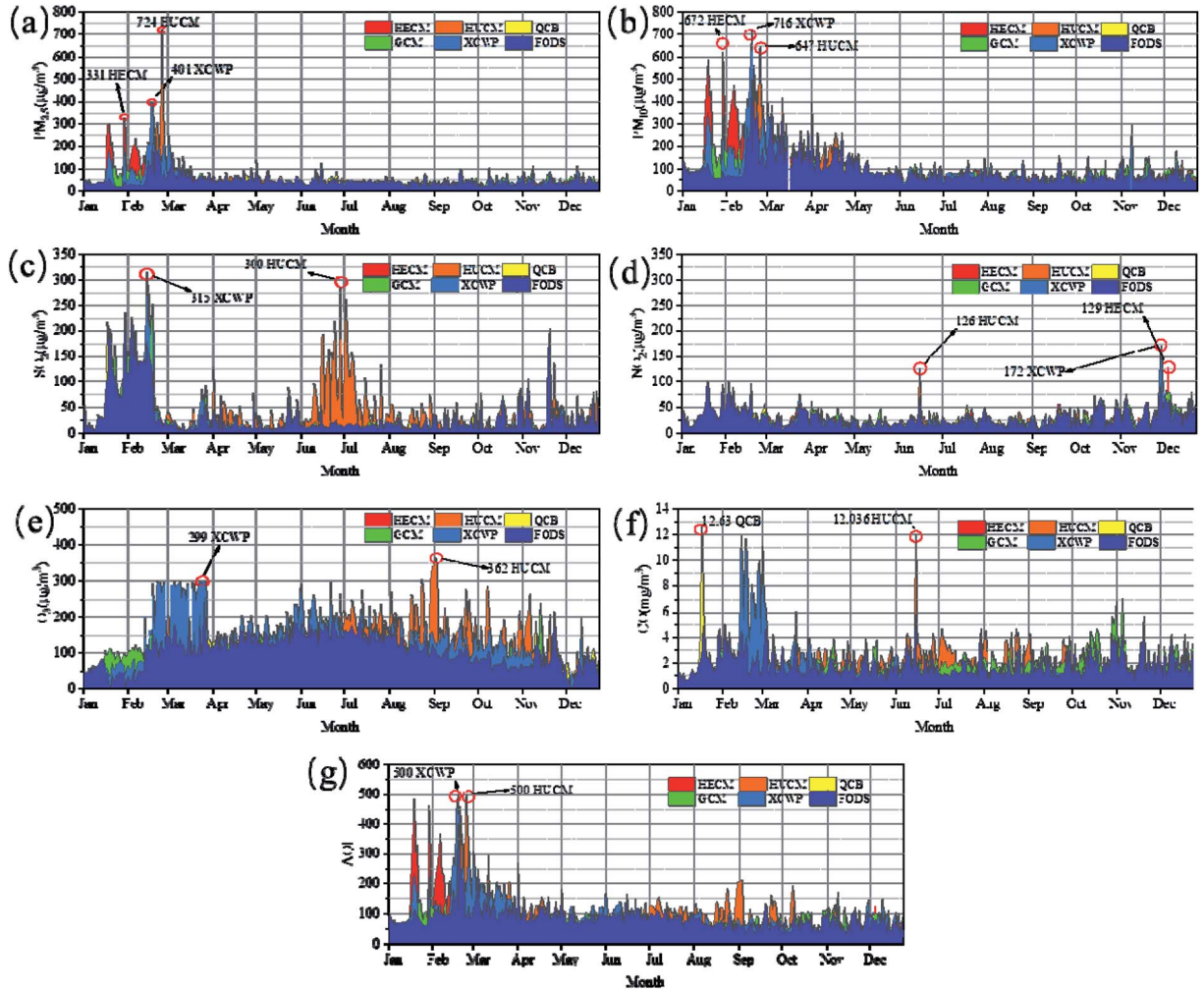

Fig. 2 Monthly variation in concentration of (a) $PM_{2.5}$, (b) PM_{10}, (c) SO_2, (d) NO_2, (e) O_3, (f) CO, and (g) AQI at six monitoring sites in 2018.

where $FS_{i,j}$ is the ith factor score of the jth monitoring sites and $FL_{k,j}$ is the factor loading, which indicates the contribution of the kth air pollutant to the jth factor.

3. Results

3.1 Daily trends and FTIR analysis

Through the analysis of the characteristics of pollutants at different observation points in the coalfield area, the trend chart of average pollutant concentration at each monitoring site in 2018 was obtained.

On February 22, the concentrations of $PM_{2.5}$ and PM_{10} were found to reach 331 μg m^{-3} and 672 μg m^{-3}, respectively, at the monitoring site of Heilonggui Coal Mine (HECM). At the Huwu Coal Mine (HUCM) and Xingyu Coal Washing Plant (XCWP) monitoring sites, the $PM_{2.5}$ concentrations on February 20 were seen to reach 724 μg m^{-3} and 674 μg m^{-3}, respectively. It can be seen from Fig. 3 that the $PM_{2.5}$ concentration is higher in spring and winter, and lower in summer and autumn.

The mean and range of O_3 found resulted in it being the most prevalent gas recorded in the atmosphere at all the six stations, followed by NO_2, SO_2, and CO, which were clearly recorded at a higher concentration at HUCM with a mean value of 102.815 μg m^{-3} (4–362 μg m^{-3}). The other gas that was also recorded at a very high concentration at HUCM was SO_2, which had an average concentration of 42.899 μg m^{-3} (3–300 μg m^{-3}).

According to the analysis of the AQI index, the highest average AQI index of HUCM was 102.8, followed by XCWP,

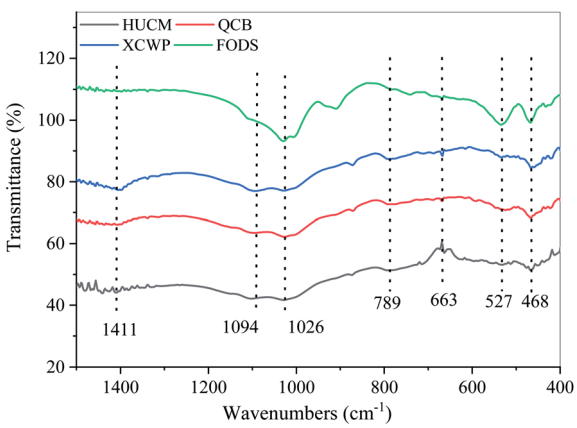

Fig. 3 FTIR spectra of $PM_{2.5}$ at four sites.

Table 1 Overall air quality data of different stations in Qipanjing with six stations as the background station

Parameters	Site	Sample number	Minimum	Maximum	Average	Standard deviation	Median
$PM_{2.5}$ ($\mu g\ m^{-3}$)	HECM	326	5	331	52.095	47.746	38.5
	HUCM	357	14	724	52.165	52.349	40
	QCB	358	13	145	40.894	19.316	37
	GCM	356	16	144	46.346	21.574	41
	XCWP	357	11	401	52.936	45.98	40
	FODS	358	15	267	44.525	27.828	39
PM_{10} ($\mu g\ m^{-3}$)	HECM	324	12	672	106.154	98.415	72
	HUCM	355	24	647	98.493	81.892	70
	QCB	357	22	292	73.036	37.21	63
	GCM	355	21	294	91.966	45.798	81
	XCWP	356	16	716	95.89	85.097	72
	FODS	356	25	559	92.126	67.642	71
SO_2 ($\mu g\ m^{-3}$)	HECM	326	3	228	27.175	38.536	15
	HUCM	357	3	300	42.899	49.439	24
	QCB	358	3	217	22.598	27.761	14
	GCM	356	2	289	26.537	36.07	15
	XCWP	356	3	315	27.587	41.335	14
	FODS	358	3	225	31.277	41.582	16
NO_2 ($\mu g\ m^{-3}$)	HECM	326	2	129	25.331	13.979	22
	HUCM	357	4	150	27.092	17.414	23
	QCB	358	1	127	25.187	15.619	21.5
	GCM	356	4	167	27.323	16.924	23
	XCWP	357	1	172	26.199	17.93	22
	FODS	358	4	103	28.399	17.521	24
CO($mg\ m^{-3}$)	HECM	326	0.568	5.097	1.421	0.739	1.19
	HUCM	357	0.622	12.036	2.111	1.13	1.981
	QCB	358	0.543	12.63	1.191	0.87	0.983
	GCM	356	0.626	7.062	2.128	0.978	1.873
	XCWP	357	0.625	11.875	2.066	1.629	1.581
	FODS	358	0.534	5.808	1.888	0.975	1.596
O_3 ($\mu g\ m^{-3}$)	HECM	326	4	290	94.549	33.074	90
	HUCM	357	4	362	136.891	62.166	136
	QCB	358	4	226	113.93	45.8	111
	GCM	356	4	240	113.093	41.632	111
	XCWP	349	4	299	140.923	67.24	134
	FODS	358	1	255	108.324	45.862	110
AQI	HECM	325	29	485	84.849	60.15	65
	HUCM	324	37	500	102.815	55.994	92
	QCB	325	31	193	77.425	24.024	75
	GCM	324	38	192	85.608	24.54	84
	XCWP	324	38	500	98.293	57.083	81
	FODS	325	34	459	88.858	41.348	84

which was 98. The average AQI index of QCB site was 77.4 and the average AQI index of the HUCM site was 1.3 times that of the QCB station. The average value of the AQI index of the other sites ranged from 84 to 88 (Table 1).

As illustrated in Fig. 2, the seasonal variation trend of SO_2 concentrations is winter (Dec, Jan, and Feb) > spring (Mar, Apr, and May) > summer (Jun, Jul, and Aug) > autumn (Sep, Oct, and Nov), which can be explained by the chemistry of SO_2 because of the lower temperature in spring and winter, and the shorter light time, the lower concentration, the lower efficiency of SO_2 conversion to SO_4^{2-}, the higher concentration of SO_2, and the lower concentration of SO_4^{2-}. In summer and autumn, when the temperature is high and the illumination time is long, the situation is just the opposite.[28] The mean concentration level in summer is the lowest but the outliers are higher than those in other seasons. The results showed that there was a high discretization in June ($18.32 \pm 15.965\ \mu g\ m^{-3}$), July ($27.78 \pm 37.271\ \mu g\ m^{-3}$), and August ($19.26 \pm 15.440\ \mu g\ m^{-3}$), indicating that the control of sulfur dioxide is complicated.

The highest concentration of NO_2 appeared in November ($36.44 \pm 17.491\ \mu g\ m^{-3}$) and December ($37.70 \pm 21.465\ \mu g\ m^{-3}$) in Fig. 2. The concentration of NO_2 displayed a significant change with different seasons and locations.

From the average monthly scale change of the AQI index, the average AQI of HECM, HUCM, and XCWP stations in February is 300. By analyzing the seasonal variation characteristics of AQI, it was found that the AQI index is the highest in spring, reaching 120 on an average, while the AQI index in the other seasons is about 100 on an average. Except for spring, the AQI index is relatively high in autumn and lowest in winter, which is 89. It can be seen that the variation trend of $PM_{2.5}$ and PM_{10} at six stations is more consistent with the trend of AQI, which indicates that the AQI has an obvious downward trend with the decrease in the fine particulate matter content.

Table 2 Statistical information on the meteorological conditions of the four seasons

Season	Spring (Mar, Apr, and May)	Summer (Jun, Jul, and Aug)	Autumn (Sep, Oct, and Nov)	Winter (Dec, Jan, and Feb)
Average high (°C)	11	30	26	3
Daily mean (°C)	4	23.5	19	3.5
Average low (°C)	−3	17	12	−10
Average precipitation (mm)	1	23	14	3
Average relative humidity (%)	30	41	46	44

Fig. 3 shows the infrared spectral characteristics of the four samples. In this analysis, we mainly pay attention to the spectra of inorganic compounds (sulfate, nitrate, and ammonium ion) that inorganic species constitute a considerable part of $PM_{2.5}$, and sulfate, nitrate and ammonium ion are the main ionic components of $PM_{2.5}$.[47,48]

Peaks at wavenumbers of 1411 cm^{-1} and 1026 cm^{-1} are NO_3^- symmetric stretching vibration and asymmetric stretching vibration, respectively. Because SO_4^{2-} in inorganic acid salt is tetrahedral, there are four vibration frequencies, which are asymmetric stretching vibration, symmetric stretching vibration, asymmetric deformation vibration, and symmetric deformation vibration, and the vibrational frequencies are located at 1094, 1026, 663, and 468 cm^{-1}, respectively. In HSO_4^-, there are two bands of S–OH stretching vibration, near 1071 and 1018 cm^{-1}, and the peaks at 1094 and 1026 cm^{-1} are their characteristic peaks, as shown in Fig. 3.

3.2 Meteorological factors

The data obtained by the air sensor were statisticed and analyzed. Multivariate analysis of variance was used to examine the effects of the monitoring sites, months, seasons, and their interactions on the concentration of different pollutants. The meteorological data from 2018, such as temperature, relative humidity, and average precipitation, were collected from the meteorological station of Qipanjing; they are expressed in Table 2. South (S) is the standard wind direction in spring (March, April, and May) and summer (June, July, and August), while north-west (N-W) and east (E) are the prevailing winds in autumn (September, October, and November) and winter (December, January, and February).

3.3 Correlation of pollutants and meteorological factors

The relationship between air pollutants and meteorological conditions was further investigated through correlation analysis. The relative humidity in summers is negatively correlated with the concentrations of pollutants $PM_{2.5}$, PM_{10}, SO_2, and NO_2, which resulted from the higher proportional humidity in summer. Macromolecular water vapor in air can easily condense to form wet precipitation, which could prevent the diffusion of atmospheric pollution.[29,30] Conversely, the humidity in winter is positively correlated with the concentration of $PM_{2.5}$, PM_{10}, SO_2, and NO_2. Therefore, the meteorological conditions of low temperature and high humidity are more conducive to liquid phase oxidation reactions and heterogeneous reactions so as to promote the formation of secondary inorganic components in $PM_{2.5}$, PM_{10}, SO_2, and NO_2, resulting in increased pollution.[31] The low-altitude inversion layer is suspended over the near-surface layer, which seriously hinders air convection. It is difficult for soot, impurities, and harmful gases suspended in the atmosphere to spread upward.[32] Wind is conducive for the diffusion and transmission of atmospheric pollutants and effectively reduces the concentration of local pollutants. Therefore, the wind speed in spring and winter has a negative correlation with the pollutants ($P < 0.01$). In summary, the pollution concentration in this area is closely related to the unfavorable meteorological conditions. Pearson's correlation coefficient (IBM SPSS21, bivariate correlation) was

Table 3 Pearson's correlation coefficients between various pollutants and meteorological parameters based on the daily average value

Season	Meteorological elements	$PM_{2.5}$	PM_{10}	SO_2	NO_2	CO	O_3
Spring	Relative humidity	−0.145	−0.099	−0.172	−0.056	−0.108	0.292[a]
	Air temperature	0.383[a]	−0.374[a]	−0.463[a]	−0.055	0.334[a]	0.421[a]
	Average wind speed	−0.097	0.027	−0.256[b]	0.282[a]	0.422[a]	0.222[b]
Summer	Relative humidity	−0.101	−0.367[a]	−0.408[a]	−0.048	0.091	0.208[b]
	Air temperature	−0.052	−0.169	0.059	0.105	−0.031	0.056
	Average wind speed	0.006	−0.065	0.083	−0.116	−0.206[b]	0.232[b]
Autumn	Relative humidity	0.387[a]	0.444[a]	0.165	0.142	−0.006	0.504[a]
	Air temperature	0.004	0.055	−0.12	0.388[a]	0.333[a]	0.729[a]
	Average wind speed	0.271[a]	−0.228[b]	−0.324[a]	0.401[a]	0.432[a]	0.085
Winter	Relative humidity	0.357[b]	0.364[b]	0.508[a]	0.310[b]	0.343[b]	0.269
	Air temperature	0.401[a]	0.478[a]	0.632[a]	−0.277	0.442[a]	0.497[a]
	Average wind speed	−0.134	−0.211	−0.142	−0.014	−0.096	−0.003

[a] Significant correlation at the 0.01 level (bilateral). [b] Significant correlation at the 0.05 level (bilateral).

used to express the association between the contaminants in each season, and each data set included the records of $PM_{2.5}$, PM_{10}, SO_2, NO_2, CO, and O_3. A two-sided correlation p also was adopted to test the local meteorological data and the results showed $p < 0.01$ for all the tests (Table 3).

Pearson's correlation matrix of four seasons in Fig. 4 shows similar patterns and dependencies in the six different monitoring sites. There are high or moderate correlations (r) between $PM_{2.5}$ or PM_{10} and NO_2 or SO_2 ($PM_{2.5}$ with NO_2: $r = 0.16$–0.45, mean $r = 0.244$; PM_{10} with NO_2: $r = 0.08$–0.44, mean $r = 0.235$; $PM_{2.5}$ with SO_2: $r = 0.11$–0.52, mean $r = 0.288$; PM_{10} with SO_2: $r = 0.07$–0.55, mean $r = 0.225$). The correlation (r) between $PM_{2.5}$ or PM_{10} and CO is stable; however, it was interesting that the correlation between $PM_{2.5}$ and CO is slightly higher ($r = 0.37$–0.59, mean $r = 0.443$) in the four seasons, and the correlation between PM_{10} and CO is the same ($r = 0.35$–0.49, mean $r = 0.408$). The correlation between $PM_{2.5}$ or PM_{10} and O_3, however, is different from other gaseous pollutants, which could be because O_3 is related to secondary aerosols and not primary aerosols.[28] The correlation between $PM_{2.5}$ or PM_{10} and O_3 was either weak or uncorrelated ($PM_{2.5}$: $r = -0.07$–0.18, mean $r = 0.09$; PM_{10}: $r = -0.11$–0.13, mean $r = 0.06$).

Due to the seasonal differences of the climatic conditions, there is a clear distinction between the correlation coefficients of the pollutants and different seasons (spring, winter, summer, and autumn). SO_2 in the atmosphere is primarily derived from the combustion emission of sulfur-containing fuels used at the coal-fired sites and in coal-burning industries. From the correlation analysis of spring and winter, there is a high correlation coefficient between $PM_{2.5}$ and PM_{10} ($r = 0.67$–0.94) and the correlation coefficient between SO_2 and $PM_{2.5}$ decreased from the spring and the winter to $r > 0.4$ compared to that of PM_{10} and CO, thereby indicating that these contaminants are from similar sources in the summer.

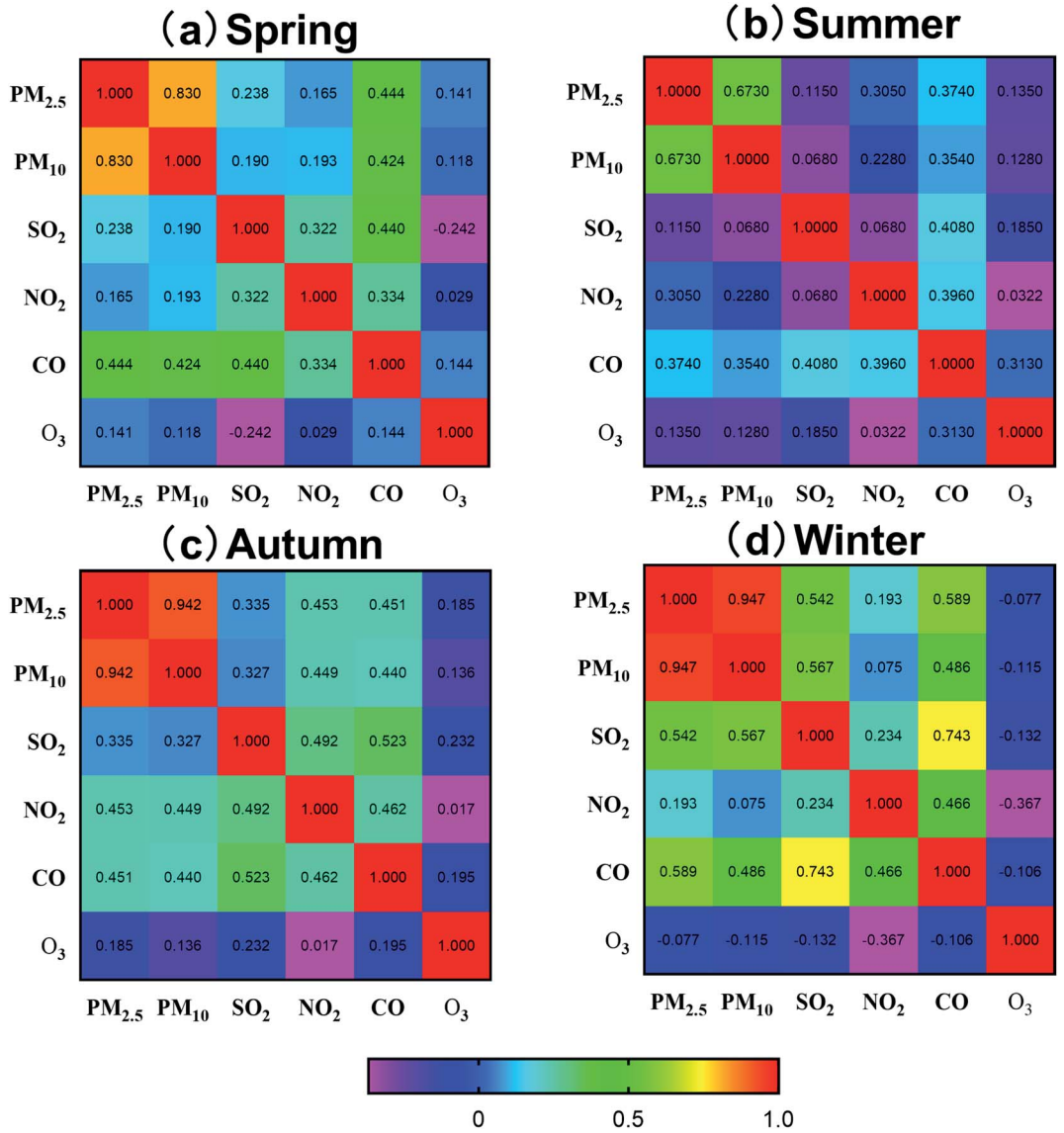

Fig. 4 The correlation matrix of the pollutants in four seasons.

3.4 Spatial variation of the pollutants

3.4.1 Concentration distribution of the pollutants. The box plots were obtained from the statistics of the six pollution-related parameters at each monitoring site, allowing the comparison of the average levels of the pollution indices and the differences in the pollution levels. The location of the monitoring points can be divided into four types—mining area, office area, dumping site, and washing coal preparation plant. Fine particles ($PM_{2.5}$) and ultra-fine particles (PM_{10}) are formed by chemical reactions such as nucleation, condensation, coagulation, evaporation of fog, and cloud droplets, in which gases also dissolve and react.[33] The primary pollutants in the mining area are PM_{10} and SO_2, which come from the accumulation of sulphide due to the spontaneous combustion of coal and the dust of coal mining. After blasting, NO and CO are usually produced in the coal mining face. When NO encounters oxygen in the air, it immediately oxidizes to NO_2.

To intuitively understand the spatial distribution characteristics of various atmospheric pollutant concentrations, the spatial interpolation analysis method is carried out for studying the pollutant concentration. The conditions in the whole studied area are illustrated in Fig. 5. It can be seen that the $PM_{2.5}$ concentration is significantly higher in the east ($48.43 \pm 31.533\ \mu g\ m^{-3}$) and west ($47.43 \pm 35.72\ \mu g\ m^{-3}$) than that in the north ($40.89 \pm 19.31\ \mu g\ m^{-3}$) and south ($46.35 \pm 21.57\ \mu g\ m^{-3}$). One of the reasons for the high concentration of $PM_{2.5}$ is that a lot of dust is produced while dumping the mining waste in the operation area. In addition, the coal dust of the coal preparation plant exhibits hygroscopicity, dispersibility, adsorption, suspension, and cohesion, which also results in the high concentration of $PM_{2.5}$. It was found that coal fire is the primary source of fine particles and ultra-fine particles in the annual average concentration distribution of various pollutants.[34] PM_{10} is also the primary pollutant in the coal field. The concentration

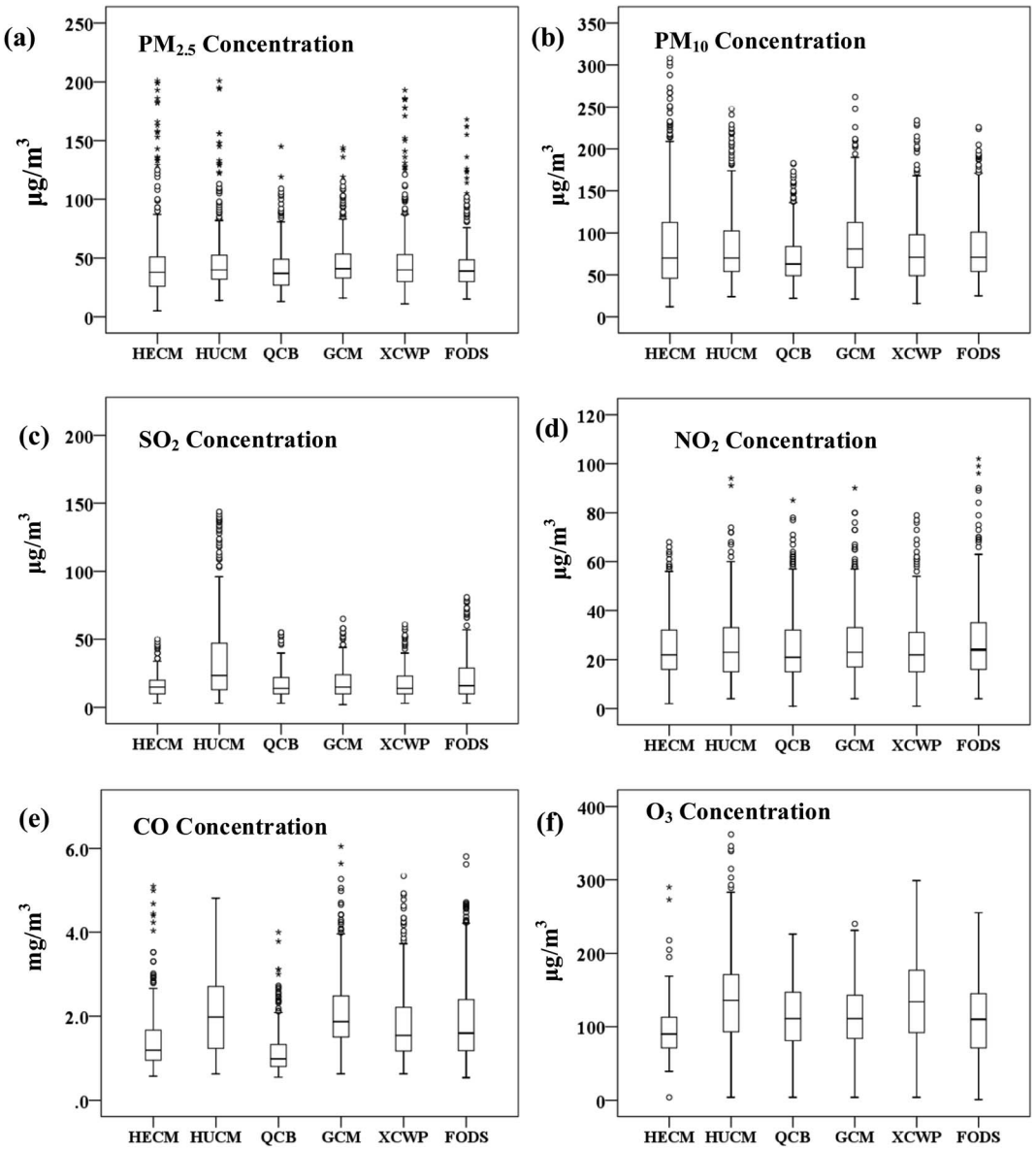

Fig. 5 Box plot of pollutants in the six monitoring sites.

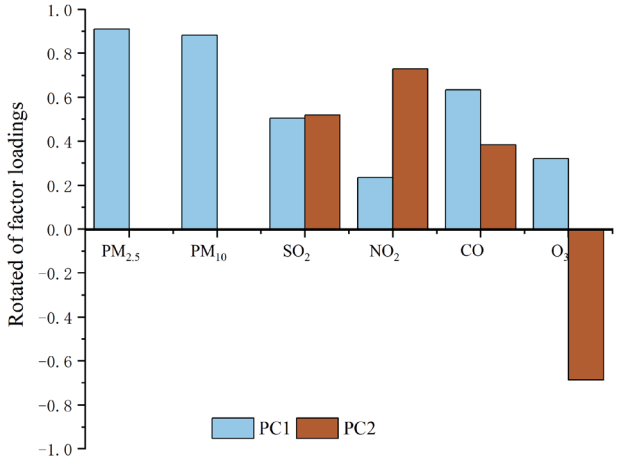

Fig. 6 Variance of rotated factor loadings in Varimax rotated principal component analysis.

of PM_{10} in the northern mining area (96.28 ± 76.07 μg m^{-3}) and coal washing plant (93.76 ± 68.52 μg m^{-3}) is higher than that in the southern office area (73.04 ± 37.21 μg m^{-3}).

3.4.2 Principal component analysis. KMO (Kaiser-Meyer-Olkin) and BTS (Bartlett's) test compares the observed correlation matrix to the identity matrix.[35] The values of KMO tests in spring, summer, autumn, and winter come to 0.735, 0.721, 0.711, and 0.740, respectively. The significance level of Bartlett's test is 0.00, which meant that the correlation matrix of the air pollutants is therefore not an identity matrix.

The air pollutant load factors are listed in Fig. 6 and Table 4. Also, there are significant characteristics in the main components, such as airborne particulate matter (PC1) and gaseous pollutants (PC2), of the pollutants at different coal mines. Therefore, all categories of pollution sources in a coal mine are identified from the marker species. The pollutants in the production areas of HUCM, GCM, and XCWP are the primary sources of PC1.

This is because the proportion of coarse particles in the air pollutants of the coal mining area is relatively high. In addition, it provides other evidence for the sources of air pollutants, *i.e.*, the primary sources of PC2 are the active burning coal or mining operation from the HECM, HUCM, GCM, and FODS.

According to the principal component scores analysis of the six monitoring points in the four seasons from Fig. 7, the monitoring in HECM, HUCM, and GCM with the highest scores in spring is mainly due to the influence of particulate matter. The monitoring points of HUCM and GCM have high scores in summer, autumn, and winter, which are mainly caused by gaseous pollutants such as particles produced by coal spontaneous combustion. QCB scored very low in all the four seasons because the monitoring point was far away from the coal mine waste dumps. The high score of the monitoring point of XCWP in spring and winter is due to the very high atmospheric stability at the monitoring point, which is not conducive for the diffusion of pollutants.

Table 4 The main components of pollutants in various mining areas of the Qipanjing monitoring sites

Site name	PC1	PC2
HECM	−0.13	0.035
HUCM	0.268	0.005
QCB	−0.348	−0.123
GCM	0.105	0.118
XCWP	0.112	−0.244
FODS	−0.005	0.218
Eigen value	2.564	1.285
Variance%	42.74	21.42
Cumulative%	42.74	64.16

4. Discussion

By analyzing the daily, monthly, and seasonal variations of atmospheric pollutant concentrations, the emissions, formation, and diffusion mechanisms of the pollutants are generalized. The higher $PM_{2.5}$ concentration is due to a large amount of coal burned for spring and winter heating supply in the northern cities and the inadequate diffusion conditions in winter. In summer, the vegetation is the lushest, the leaf area of the green plants is significantly increased, and the leaves with a rough surface are favorable for the capture of $PM_{2.5}$, which makes it easy to reduce the $PM_{2.5}$ concentration.[24] Previous studies have shown that meteorological factors, such as the temperature, rainfall, and wind speed have a significant impact on the spatial and temporal distribution of $PM_{2.5}$ and PM_{10} concentrations in the atmosphere.[23]

The coal seams or gangue hills burn away from the atmosphere by surface dry sedimentation or oxidation to sulphate. The oxidation of SO_2 in the atmosphere can occur homogeneously in the gas phase and the aqueous phase (raindrops), heterogeneously on the surfaces of particles, or simultaneously through all three processes.[36] The oxidation rate of SO_2 from burning coal in summer is higher than that in winter but the dry deposition rate of SO_2 in winter is higher than that in summer.[22] The main component of NO_x released from the coal fire area is NO, which then further reacts in the air to form NO_2. In addition, automobile exhaust emissions in the mining area was paid close attention to and some NO_x emissions produced during the ignition and combustion process of fuel.[26] The seasonal variation in the NO_2 concentration mainly depends on the meteorological conditions at different days in the year. Also, in the absence of sunlight, NO_2 has a longer life in the atmosphere,[37] which explains why NO_2 is higher in winter. It is difficult to maintain gas mixing at their interface in winter, leading to an increase in the NO_2 levels during this season.[38]

The large-scale use of coal in spring and winter has led to a significant increase in pollutant emissions. Meanwhile, severe weather conditions will further aggravate pollution.[39] O_3 has a negative correlation between the concentration of NO_2 and CO, which is consistent with the previous findings, *i.e.*, these pollutants, similar to some other volatile organic compounds, are considered as the chemical precursors of O_3. Furthermore, the meteorological conditions also play a crucial role in the photochemical processes that affect the formation and destruction of O_3.[40,41] Pearson coefficient analysis shows that

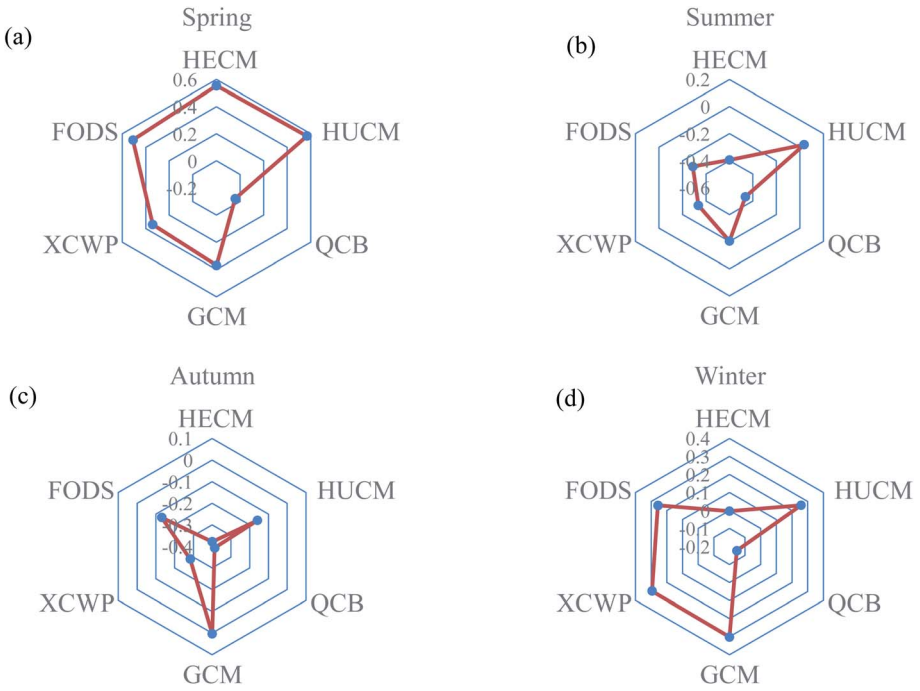

Fig. 7 Relative plot of PCS in the four seasons including the six monitoring sites.

there is no significant difference between the $PM_{2.5}$ and PM_{10} coefficients in the same season but the difference in the same gaseous pollutant in different seasons is very significant. There is a significant positive correlation between $PM_{2.5}$ and PM_{10}, while NO_2 and SO_2 all present a notable negative correlation with wind speed and the correlation degree is -0.05.

Wind speed, relative humidity, temperature, and rainfall are the control parameters for the seasonal variations of air pollutant concentration in the area. The average concentrations of airborne particulate matter and gaseous pollutants in the air were calculated based on the daily data of air pollutants monitored at the study sites. Since there were many fire hotspots from March 8 to 13 (Fig. 8), the distribution of the pollutants in the 5 days were analyzed. The $PM_{2.5}$ concentration was higher than 100 $\mu g\ m^{-3}$ from March 11 to 13. The number of fire points on the 10th reached 56, which was in good agreement with the most serious gas pollution in the area. The trend of CO was similar to $PM_{2.5}$. On March 10, the concentration of CO reached 95 $mg\ m^{-3}$ and the concentration of SO_2 also reached 94 $\mu g\ m^{-3}$. In the next few days, the concentration of SO_2 remained above 60 $\mu g\ m^{-3}$ because SO_2 was the main gas emitted during the spontaneous combustion of the coalfield.

The HYSPLIT trajectory model was used to simulate the 24 hour transport of pollutants in the process of serious pollution from March 8 to 13, 2018. The height limits of the air masses are set at 100 m, 500 m, and 1000 m, representing the ascending range of the bottom, middle, and upper air masses, respectively. The latitude and longitude of the area is selected as the end point of the backward trajectory. The simulation results are shown in Fig. 8. It can be seen that the most of the bottom air masses come from the northwest and the air masses on March 10 originate from the south. The short trajectory of the air mass indicates the slow movement. The maximum distribution height of the air masses does not exceed 1000 m, indicating that the wind is less, the wind speed is slow, and the pressure difference is small, which prevents the vertical diffusion of pollutants. These air masses carry the pollutant gases and particulates produced by the spontaneous combustion of coal gangue, which further increases the pollution level in this area. By March 14, the three airflow trajectories were basically close to the situations on March 10 and the diffusion conditions were restored to their previous state. The concentration of pollutants in this area is greatly affected by the increase in the spontaneous combustion points and the transmission process of the pollutants inevitably affects this area.

The spatial distribution difference of SO_2 concentration in the western area is higher than that in the eastern area. The generation of SO_2 may be attributed to the active coal fires in the mining area and the hard coke industry. There was no significant difference in the total concentration of NO_2 and that (28.19 ± 17.09 $\mu g\ m^{-3}$) of the northern area was slightly higher than that of the southern area (24.90 ± 14.67 $\mu g\ m^{-3}$). Similarly, the difference in the CO concentration in the various places on the studied area was not obvious. Only a slightly higher concentration of CO was found in the northeast; one of the main reasons was that there is a main road nearby, and more CO was produced by the emissions of motor vehicles on it. The concentration of O_3 in the studied area showed a trapezoid, increasing gradually from north to south, and the relatively high concentration appeared in a high-altitude zone. The generation of O_3 was influenced by the comprehensive factors, such as sectional illumination, temperature, and other meteorological conditions, as well as local emission sources and regional

pollutant transport. The photochemical reaction was the main way to increase O_3 in the near surfaces.[42] Studies have shown that poisonous emissions and particulate matter are emitted by coal mine fires, resulting in poor air quality and having a direct effect on the people who normally live near coal mines. The data will need to be extrapolated to other mine fires with caution as the properties of coal can differ greatly spatially and temporally.[43–46]

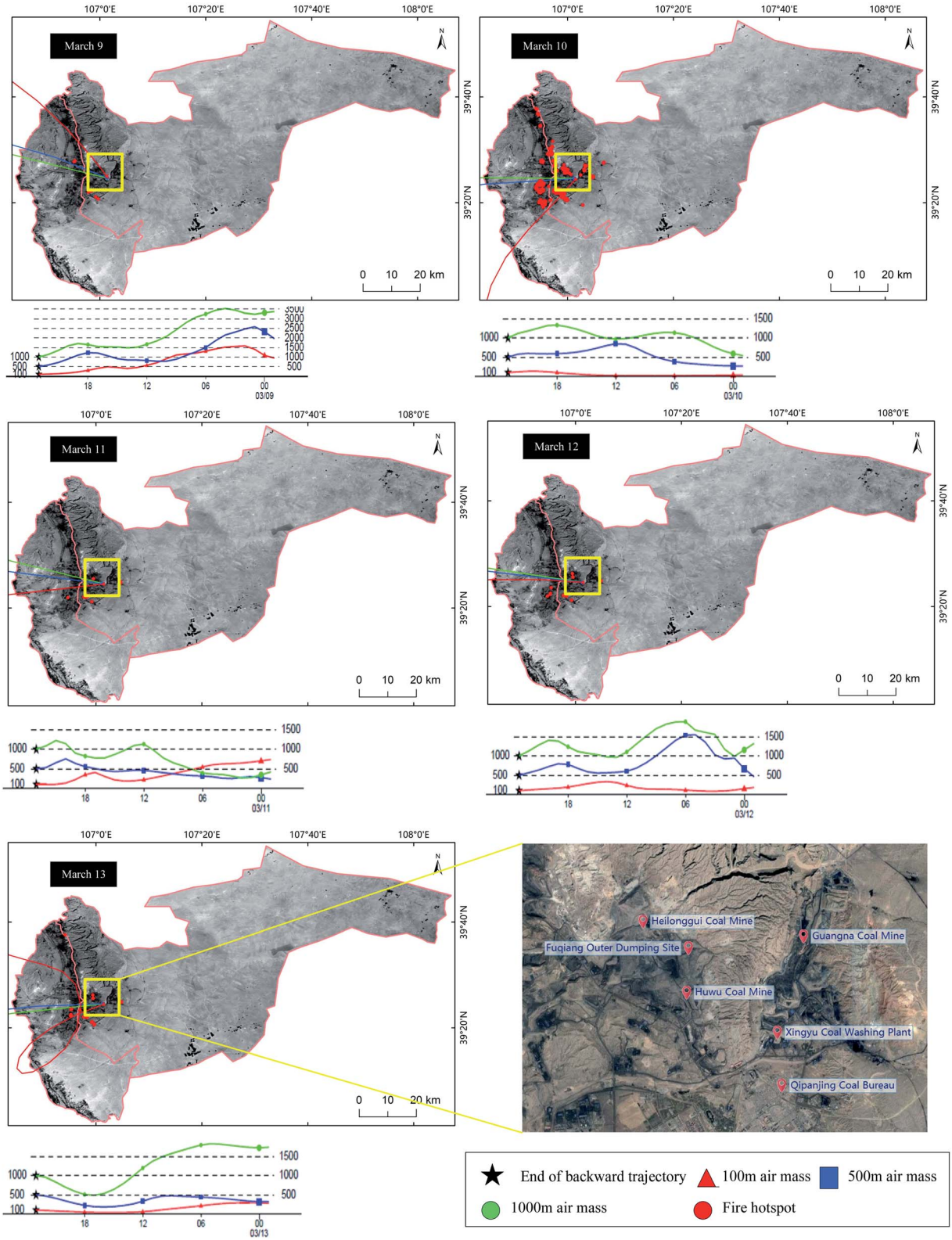

Fig. 8 Fire hotspot distribution and HYSPLIT trajectory model from March 8 to 13 in the studied area.

5. Conclusion

In this study, taking the Qipanjing area of Ordos city as an example, the one-year monitoring of pollutants, including $PM_{2.5}$, PM_{10}, SO_2, NO_2, O_3, and CO, was conducted based on the exposure level of coalfield fires and industrial mines. There is a positive correlation between $PM_{2.5}$, PM_{10}, and SO_2, whereas the O_3 concentrations are negatively correlated with these pollutants. Through principal component analysis, it was recognized that coal mining and active coal gangue fires (42.74% change) are significant contributors to the air pollutants of the studied region. Gaseous pollutant emissions (21.42% change) are another cause of the deterioration in the air quality around the coal mines. It is argued that reducing pollutant emission is the key to resolving the issues of coalfield pollution.

Abbreviations

FTIR	Fourier transform infrared spectroscopy
PM_{10}	Particulate matter 10 μm
$PM_{2.5}$	Particulate matter 2.5 μm
SO_2	Sulphur dioxide
NO_2	Nitrogen dioxide
CO	Carbon monoxide
O_3	Ozone
H_2S	Hydrogen sulfide
NO_x	Nitrogen oxides
NH_3	Ammonia
HECM	Heilonggui Coal Mine
HUCM	Huwu Coal Mine
GCM	Guangna Coal Mine
FODS	Fuqiang Outer Dumping Site
XCWP	Xingyu Coal Washing Plant
QCB	Qipanjing Coal Bureau

Conflicts of interest

There are no conflicts to declare.

Acknowledgements

The study is financially supported by Major Program of National Natural Science Foundation of China (No. 72091512 and 71790613). And Major science and technology project of Inner Mongolia Autonomous Region under Grant No. RZ190001148. The authors appreciate the supports deeply.

References

1 S. M. Melody and F. H. Johnston, *Int. J. Coal Geol.*, 2015, **152**, 1–14.
2 K. Brown, *Science*, 2003, **299**, 1177.
3 C. Kuenzer, J. Zhang, A. Tetzlaff, P. van Dijk, S. Voigt, H. Mehl and W. Wagner, *Appl. Geogr.*, 2007, **27**, 42–62.
4 Z. Song and C. Kuenzer, *Int. J. Coal Geol.*, 2014, **133**, 72–99.
5 P. Van Dijk, J. Zhang, W. Jun, C. Kuenzer and K.-H. J. Wolf, *Int. J. Coal Geol.*, 2011, **86**, 108–119.
6 X. Querol, M. Izquierdo, E. Monfort, E. Álvarez, O. Font, T. Moreno, A. Alastuey, X. Zhuang, W. Lu and Y. J. Wang, *Int. J. Coal Geol.*, 2008, **75**, 93–104.
7 R. Finkelman, *Potential health impacts of burning coal beds and waste banks*, 2004.
8 Y. Liang, H. Liang and S. Zhu, *Atmos. Environ.*, 2014, **83**, 176–184.
9 G. B. Stracher and T. P. Taylor, *Int. J. Coal Geol.*, 2004, **59**, 7–17.
10 C. Künzer, *Demarcating coal fire risk areas based on spectral test sequences and partial unmixing using multi sensor remote sensing data*, 2004.
11 Y. Zhao, J. Zhang, C. L. Chou, Y. Li, Z. Wang, Y. Ge and C. Zheng, *Int. J. Coal Geol.*, 2008, **73**, 52–62.
12 J. N. Carras, S. J. Day, A. Saghafi and D. J. Williams, *Int. J. Coal Geol.*, 2009, **78**, 161–168.
13 X. Hong, H. Liang, L. Shuai, Y. Jia, T. Zhao, W. Liang, X. Hong, H. Liang, L. Shuai and Y. Jia, *Int. J. Coal Geol.*, 2017, **181**, 78–86.
14 Ö. Özden, T. Döğeroğlu and S. Kara, *Environ. Int.*, 2008, **34**, 678–687.
15 A. Bytnerowicz, B. Godzik, W. Fraczek, K. Grodzińska, M. Krywult, O. Badea, P. Barančok, O. Blum, M. Cerny, S. Godzik, B. Maňkovská, W. Manning, P. Moravcik, R. Musselman, J. Oszlanyi, D. Postelnicu, J. Szdzuj, M. Varsavova and M. Zota, *Environ. Pollut.*, 2002, **116**, 3–25.
16 M. Yadav, S. P. Sahu and N. K. Singh, *J. Clean. Prod.*, 2019, **207**, 97–110.
17 L. Matějíček, P. Engst and Z. Jaňour, *Ecol. Model.*, 2006, **199**, 261–277.
18 R. Romanowicz, P. Young, P. Brown and P. Diggle, *Environ Model Softw.*, 2006, **21**, 759–769.
19 C. de Fouquet, D. Gallois and G. Perron, *Atmos. Environ.*, 2007, **41**, 6701–6714.
20 R. Betha, M. Pradani, P. Lestari, U. Joshi, J. Reid and R. Balasubramanian, *Atmos. Res.*, 2013, **122**, 571–578.
21 A. Valavanidis, K. Fiotakis and T. Vlachogianni, *J. Environ. Sci. Health, Part C: Environ. Carcinog. Ecotoxicol. Rev.*, 2008, **26**, 339–362.
22 C. Pio and M. S. Feliciano, *Phys. Chem. Earth*, 1996, **21**, 373–377.
23 Z. Liu, B. Hu, L. Wang, F.-K. Wu, W. Gao and Y. Wang, *Environ. Sci. Pollut. Res.*, 2015, **22**, 627–642.
24 D. J. Nowak, S. Hirabayashi, A. Bodine and R. Hoehn, *Environ. Pollut.*, 2013, **178**, 395–402.
25 M. D. Petters and S. Kreidenweis, *A single parameter representation of hygroscopic growth and cloud condensation nuclei activity*, 2007.
26 Z. Hao, H. Yan, G. Mo, Z. Liao and K. Cen, *J. Energy Inst.*, 2015, **90**, S1743967115300520.
27 D. Xu, X. Kang, Z. Liu, D. Zhuang and J. Pan, *Sci. China, Ser. D: Earth Sci.*, 2009, **52**, 855–868.
28 A. K. Tripathi and M. Gautam, *J. Environ. Biol.*, 2007, **28**, 127–132.

29 F. J. Brechtel and S. M. Kreidenweis, *J. Atmos. Sci.*, 2000, **57**, 1872.
30 M. Alghamdi, M. Khoder, R. Harrison, A. P. Hyvärinen, T. Hussein, H. Al-Jeelani, A. S. Abdelmaksoud, M. H. Goknil, I. Shabbaj, F. M. Almehmadi, H. Lihavainen and K. Hämeri, *Atmos. Environ.*, 2014, **94**, 205–214.
31 Y. L. Sun, Q. Zhang, J. J. Schwab, W. N. Chen, M. S. Bae, Y. C. Lin, H. M. Hung and K. L. Demerjian, *Atmos. Chem. Phys.*, 2011, **11**, 25751–25784.
32 S. Wang and L. M. Polvani, *J. Geophys. Res.: Atmos.*, 2011, **116**, D5.
33 S.-S. Tsai, C.-C. Chang, s.-h. Liou and C.-Y. Yang, *Int. J. Environ. Res. Public Health*, 2014, **11**, 5081–5093.
34 R. S. Vedala, R. C. Karra, K. V. Nagesha, E. Muralidhar and M. Shoeb Mohiuddin, *Procedia Earth Planet. Sci.*, 2015, **11**, 303–311.
35 J. Zhang, L.-y. Zhang, M. Du, W. Zhang, X. Huang, Y.-q. Zhang, Y.-y. Yang, J.-m. Zhang, S.-h. Deng and F. Shen, *Atmos. Environ.*, 2016, **144**, 37–46.
36 B. Pandey, M. Agrawal and S. Singh, *Atmos. Pollut. Res.*, 2014, **5**, 79–86.
37 L. Li, C.-H. Chen, C. Huang, H.-Y. Huang, Z.-P. Li, J. Fu, C. J Jang and D. G. Streets, *Regional air pollution characteristics simulation of O3 and PM10 over Yangtze River Delta region*, 2008.
38 X. Yang, S. Wang, W. Zhang, D. Zhan and J. Li, *The impact of anthropogenic emissions and meteorological conditions on the spatial variation of ambient SO2 concentrations: A panel study of 113 Chinese cities*, 2016.
39 Y. Sarbassov, L. Duan, V. Manovic and E. Anthony, *Greenhouse Gases: Sci. Technol.*, 2018, **8**, 402–428.
40 R. García, A. Stohl, K. Karatzas, T. Bohler, P. James and J. Camaño, *Environ Model Softw.*, 2005, **20**, 587–593.
41 Y. Yan, L. Peng, R. Li, Y. Li, L. Li and H. Bai, *Environ. Pollut.*, 2017, **223**, 295–304.
42 J.-d. Li, Q.-h. Deng, C. Lu and B.-l. Huang, *J. Cent. South Univ. Technol.*, 2010, **17**, 509–515.
43 S. Mondal, G. Singh and M. K. Jain, *Environ. Monit. Assess.*, 2020, **192**, 405.
44 J. Ribeiro, E. F. da Silva and D. Flores, *Int. J. Coal Geol.*, 2010, **81**, 359–372.
45 F. Reisen, R. Gillett, J. Choi, G. Fisher and P. Torre, *Atmos. Environ.*, 2017, **151**, 140–151.
46 X. Querol, M. Izquierdo, E. Monfort, E. Álvarez, O. Font, T. Moreno, A. Alastuey, X. Zhuang, W. Lu and Y. Wang, *Int. J. Coal Geol.*, 2008, **75**, 93–104.
47 A. Reff, B. J. Turpin, R. J. Porcja, R. Giovennetti, W. Cui, C. P. Weisel, *et al.*, *Indoor Air*, 2005, **15**(1), 53–61.
48 J. H. Liu, Y. H. Zhang, L. Y. Wang and Z. F. Wei, *Spectrochim. Acta, Part A*, 2005, **61**(5), 893–899.